Research Article

Ion exchange synthesis of Ag^{+} incorporated $LiAlO_2$ and its application in photodegradation of organic dyes

Ravi Gundeboina[1] · **Vithal Muga**[1]

Abstract

The present work aimed at the synthesis, characterization and photodegradation studies of visible light active silver ion (Ag^{+}) incorporated $LiAlO_2$ catalyst. Ethylene glycol assisted sol–gel method was adopted to prepare $LiAlO_2$ at 700 °C. $AgAlO_2$ was synthesized by cation exchange of $LiAlO_2$ by the solid-state method at 300 °C. The structural and optical properties were characterized by powder X-ray diffraction and UV–Vis diffuse reflectance spectroscopy respectively. The scanning electron microscopy (SEM) provided the morphological information of as-prepared samples. $LiAlO_2$ and $AgAlO_2$ were crystallized in a tetragonal lattice (space group $P4_12_12_1$) and orthorhombic (space group Pna21) respectively. The bandgap energy of the samples was determined by the Kubelka–Munk (KM) plot. SEM measurements revealed the flower-like hierarchical shape particles. The photocatalytic properties of these samples were evaluated by the degradation of methylene blue and rhodamine B dyes. The mechanistic degradation pathway of RhB was studied using radical quenchers. The rate of recombination of the charge carriers during photocatalysis was discussed.

Graphical abstract

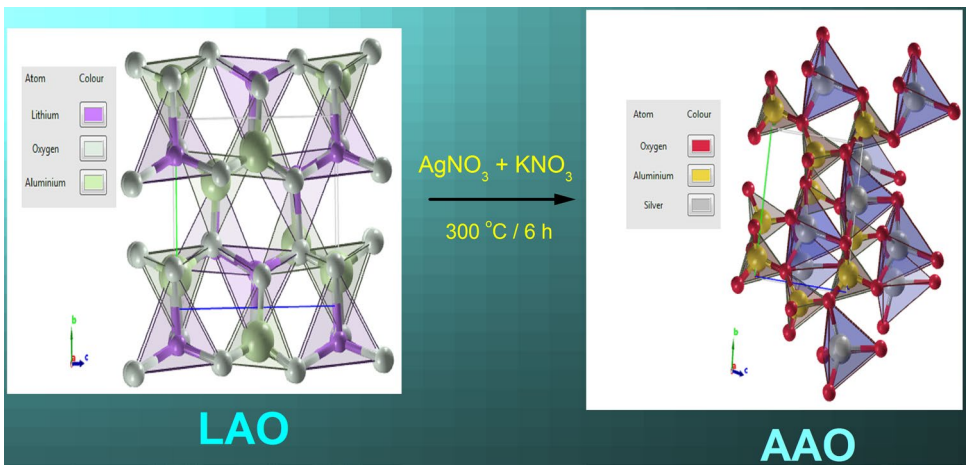

Keywords $LiAlO_2$ · $AgAlO_2$ · Powder XRD · Morphology · Photodegradation

✉ Vithal Muga, muga_vithal@rediffmail.com | [1]Department of Chemistry, University College of Science, Osmania University, Hyderabad 500007, India.

SN Applied Sciences (2019) 1:164 | https://doi.org/10.1007/s42452-019-0166-4

Received: 10 October 2018 / Accepted: 4 January 2019 / Published online: 14 January 2019

1 Introduction

The increase in pollution due to civilization and development in human activities cause global warming and health disorders. Particularly, water pollution because of dumping of industrial wastes into the rivers and other water bodies instigate an imbalance in the water resulting in severe contamination and death of aquatic species. Thus, there is a necessity to curb water pollution through cost-effective scientific methods. Semiconductor mediated photocatalysis has attracted the attention of scientific industry due to its broad applications in the decomposition of environmental pollutants and production of clean hydrogen energy [1–5]. The researchers successfully synthesized a large number of semiconducting materials for the degradation of organic contaminants present in water and air. However, many of these materials respond to UV light only due to their wide bandgap energy (E_g) higher than 3.2 eV. Since only about 4–5% of the solar spectrum falls in the UV range, extensive research has been carried out to investigate the visible light sensitive oxide semiconductors in view of the better utilization of solar energy or indoor artificial illuminations [6–10]. Modification of band edge (valence band or conduction band) position of wide bandgap energy (E_g) materials by doping of cation/anion into their lattice is one of the strategies to make them visible-light sensitive photocatalysts [11, 12]. Noble metals such as platinum (Pt), silver (Ag) and gold (Au) substituted semiconductors have paid more attention mainly in heterogeneous photocatalysis due to their remarkable photocatalytic properties [13, 14]. The *d*-orbitals of these metals can hybridize with the O 2*p* orbitals in the valence band of material, increasing the energy of valence band maximum and results in a decrease in E_g.

Silver-based oxides have been used as efficient photocatalysts for the degradation of organic dyes [6, 15, 16]. Thus, the design and development of visible light active photocatalyst, $AgAlO_2$, has been chosen. However, the direct preparation of silver-based oxides by the solid-state reaction encountered practical problems due to the decomposition of Ag_2O to elemental Ag at higher temperature [17]. A process employing a cation exchange reaction has been chosen for the preparation of Ag-based oxides. Hence, in the present investigation, $AgAlO_2$ is prepared from $LiAlO_2$ by cation exchange solid reaction process. To the best of our knowledge, synthesis of a flower-like hierarchical β-$AgAlO_2$ and its photocatalytic activity against methylene blue (MB) and rhodamine B (RhB) degradation studies under visible light irradiation have not been reported. The structure and photocatalytic properties of $LiAlO_2$ and $AgAlO_2$ are studied and compared.

2 Experimental

2.1 Synthesis of $LiAlO_2$

Lithium aluminum oxide, $LiAlO_2$, is prepared using the sol–gel method.

Solution "A": Stoichiometric amount of $LiNO_3$ was dissolved in 15 ml of double distilled water.

Solution "B": Calculated amount of $Al(NO_3)_3.9H_2O$ was dissolved in 15 ml of double distilled water.

The solution A is mixed with solution B. Aqueous citric acid solution was added to the mixture such that the mole ratio of citric acid to metal ion was 2:1. The pH of the resultant metal citrate solution was adjusted to 6–7 by dropwise addition of dilute ammonia solution. The solution was then slowly evaporated on a magnetic stirrer till a viscous liquid was obtained. At this stage ethylene glycol (gelating reagent) was added (mole ratio of citric acid to ethylene glycol was 1:1.2). This mixture was heated on a hot plate at 100 °C for 2–3 h. The temperature was increased to 160–180 °C to obtain a fluffy solid material. This material was ground in an agate mortar using spectral grade acetone and heated to about 300-400 °C in small amounts in an electric burner to obliterate the organic matter. The resultant ash colored solid (precursor) was heated in a muffle furnace at 700 °C temperature for 14 h to obtain the desired $LiAlO_2$ (heat after named as LAO).

2.2 Synthesis of $AgAlO_2$

LAO powder was mixed with $AgNO_3$ and KNO_3 in the molar ratio of 1:2:3 in an agate mortar. Here, the KNO_3 is used as a flux. This mixture was crushed thoroughly for 60 min and heated in air at 300 °C for 6 h. The resultant mixture was washed with distilled water to remove unreacted reactants. This material was dried in air at 60 °C and labeled as AAO.

2.3 Characterization

Powder X-ray diffraction (PXRD) data for a sample was collected using a Philips X pert pro X-ray diffractometer with Cu Kα radiation with a scan speed of 0.02 degrees/sec. FT-IR spectral analysis was carried out by Shimadzu spectrometer using KBr pellets. The SEM images were taken on a HITACHI SU-1500 variable pressure scanning electron microscope. The UV–Vis diffuse reflectance spectra (UV–Vis DRS) of the samples were recorded using JASCO V-650 UV–Vis spectrophotometer and $BaSO_4$ was used as reference material. Reflectance spectra were collected in the wavelength range 900–200 nm. The reflectance was transformed into the Kubelka–Munk (KM) function. Photon

energy at the absorption edge was estimated by extrapolating the linearly ascending portion of the spectrum to the x-axis, and the value was defined as an optical bandgap. The photoluminescence spectra are recorded with a JASCO FP-8500 spectrofluorometer.

2.4 Photocatalytic activity measurements

The photocatalytic activity of as-synthesized catalysts was tested using HEBER visible annular type photoreactor equipped with a 300 W Tungsten lamp (wavelength range 380–840 nm). In the experiment, 50 ml of 10^{-5} M aqueous MB (or RhB) solution comprising of 50 mg of AAO (or LAO) catalyst is aerated in darkness for 60 min to achieve the adsorption–desorption equilibrium. Then, the resultant solution was illuminated by a 300 W Tungsten lamp and collected aliquots of the aqueous dye solution at regular 30 min intervals. The absorbance of illuminated dye samples was recorded using a spectrophotometer. The MB (or RhB) degradation efficacy has been determined as follow

$$Degradation\ (\%) = \frac{C_0 - C_t}{C_0} \times 100$$

where C_0 and C_t are the absorbance of MB (or RhB) solution before and after photoirradiation with a UV–Vis spectrophotometer.

2.4.1 Mechanistic photodegradation pathway studies

Controlled photocatalytic experiments using different radical scavengers were carried out under similar experimental conditions to realize the mechanism of photocatalytic degradation of RhB in the presence of AAO. The reaction mixture consists of 3 mL of 2 mM scavenger, 50 mL of RhB and 0.05 g of catalyst. Ammonium oxalate (AO), benzoquinone (BQ) and isopropanol (IPA) were used as scavengers for photogenerated holes, superoxide radical and hydroxyl radical species, respectively.

3 Results and discussions

High-temperature (> 900 °C) preparation of $LiAlO_2$ and its crystal structure has been studied by many authors [18–20]. In the present investigation, LAO is prepared at 700 °C using the sol–gel method. It is subjected to PXRD to identify its phase purity. The powder patterns of this sample are well matched with that of γ-$LiAlO_2$ [JCPDF: 73-1338] (Fig. 1). Thus, LAO was crystallized in tetragonal structure with space group $P4_12_12_1$. The structure of this phase is shown in Fig. 2a. In this structure, Li and Al are tetrahedrally coordinated to four oxygen atoms such

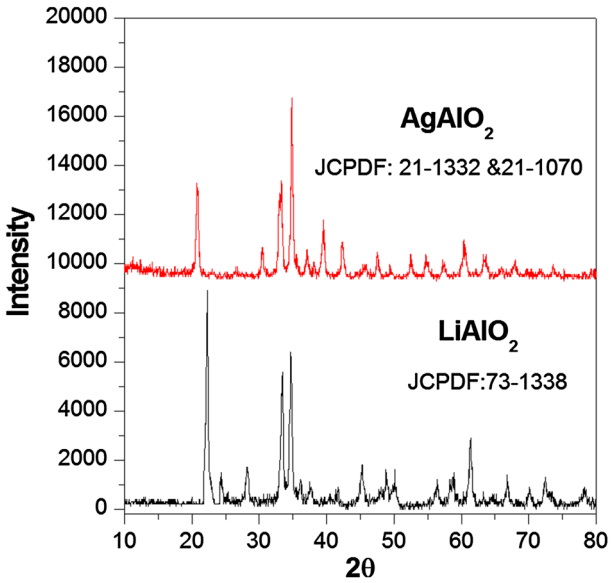

Fig. 1 The powder XRD patterns of LAO and AAO

that O-edge shared LiO_4 and AlO_4 tetrahedra and O-corner shared LiO_4–AlO_4 pairs. Besides this tetragonal form, $LiAlO_2$ has two other forms, α and β, which are crystallized in trigonal and orthorhombic structures respectively. The phase of the LAO depends on its sintering temperature. At lower temperatures, α and β $LiAlO_2$ phases were obtained beside γ-$LiAlO_2$ [21].

An X-ray diffraction pattern of ion exchanged product is consistent with β-$AgAlO_2$ (JCPDF No. 21-1332 & 21-1070) (Fig. 1). It is reported that $AgAlO_2$ crystallizes in delafossite structure (rhombohedral system with the space group $R\bar{3}m$) or cristobalite related structure (an orthorhombic system with the space group Pna21) [22, 23]. The formation of these forms depends on the starting materials and method of preparation [22–24]. The crystal structure of AAO is shown in Fig. 2b. The lattice parameters of both samples are determined using Powd software by least square fitting of their d-lines. The obtained values are close to that of reported values and given in Table 1. In this structure each atom is tetrahedrally coordinated i.e., the structure can be described as corner shared AgO_4, AlO_4, and OAg_2Al_2 tetrahedra.

The scanning electron microscopy (SEM) images of LAO and AAO powders measured in different magnifications (2 µm, and 1 µm) are shown in Fig. 3. It is found to be that both the samples have flower-like hierarchical shapes. The optical properties of these samples are studied by UV–visible diffused reflectance spectra (Fig. 4). The absorption edge of LAO and AAO was observed in UV (340–360 nm) and visible (550–600 nm) regions respectively. The bandgap energy (E_g) of the semiconductor is related to its band edge. The ionic radius of

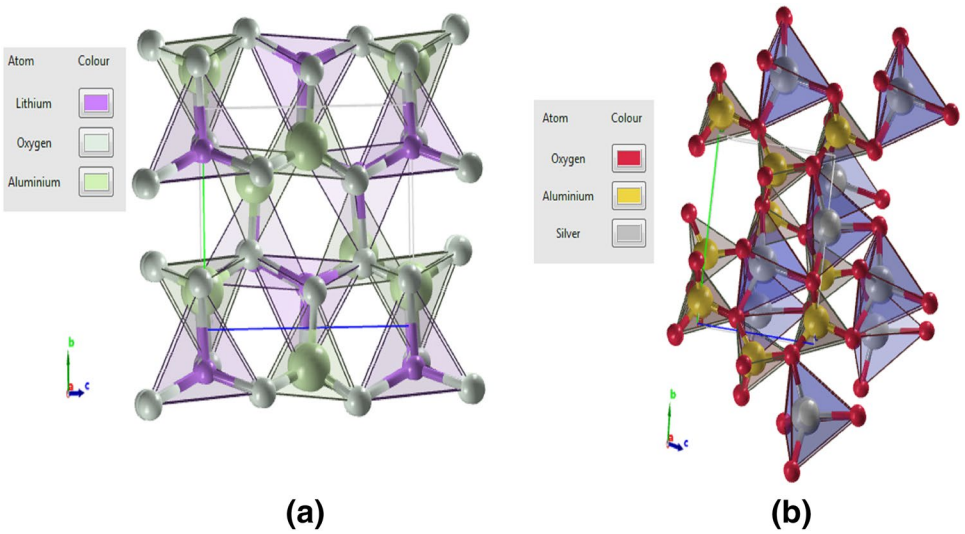

Fig. 2 The schematic structures of **a** γ-LAO and **b** β-AAO

Table 1 Unit cell parameters of LAO and AAO

	A (Å)	B (Å)	C (Å)	α°	β°	γ°
LAO	5.159	5.159	6.283	90	90	90
AAO	5.426	6.975	5.381	90	90	90

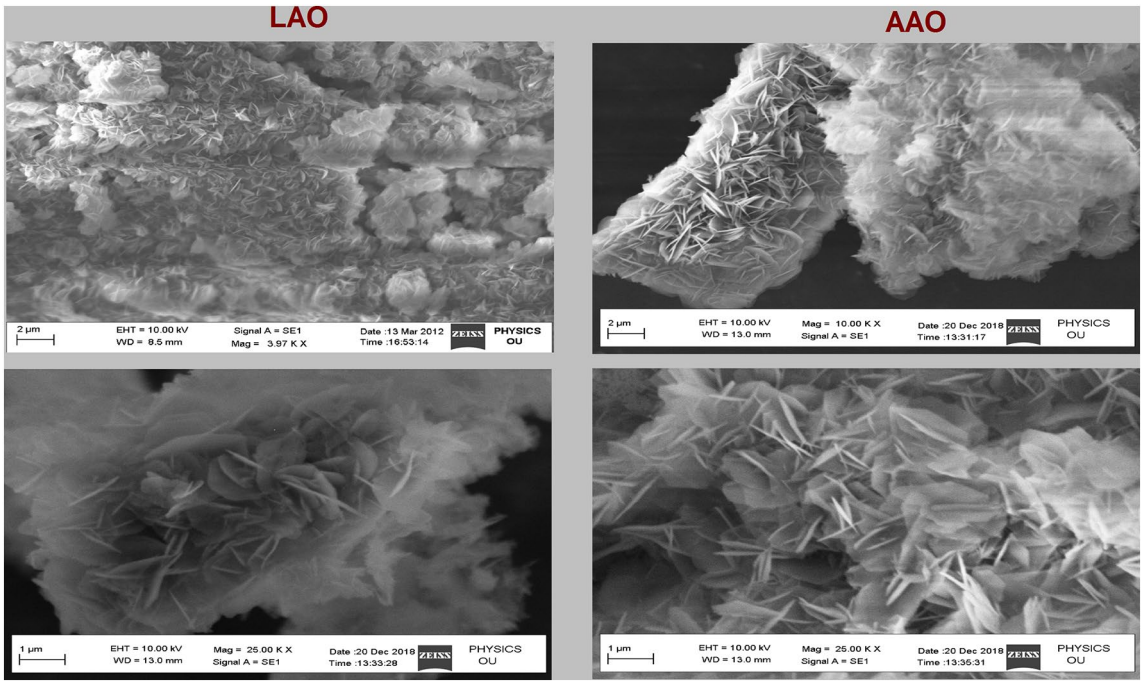

Fig. 3 SEM images of LAO and AAO

the dopant and the host cations, as well as the chemical nature of the dopants, will influence the relative shift of the absorption edge of the semiconductor [25]. The bandgap energy of the oxides, LAO and AAO, can be obtained from the Kubelka–Munk (KM) plot of $(Khv)^{1/2}$ versus hv, where K is reflectance transformed according to Kubelka–Munk [$K = \frac{(1-R)^2}{2R}$, where R is reflectancy (%)] and hv is photon energy (Fig. 4). Extrapolation of the linear portion of the plot to $(Khv)^{1/2} = 0$ (i.e., onto the x-axis) gives an estimation of bandgap energy. The bandgap

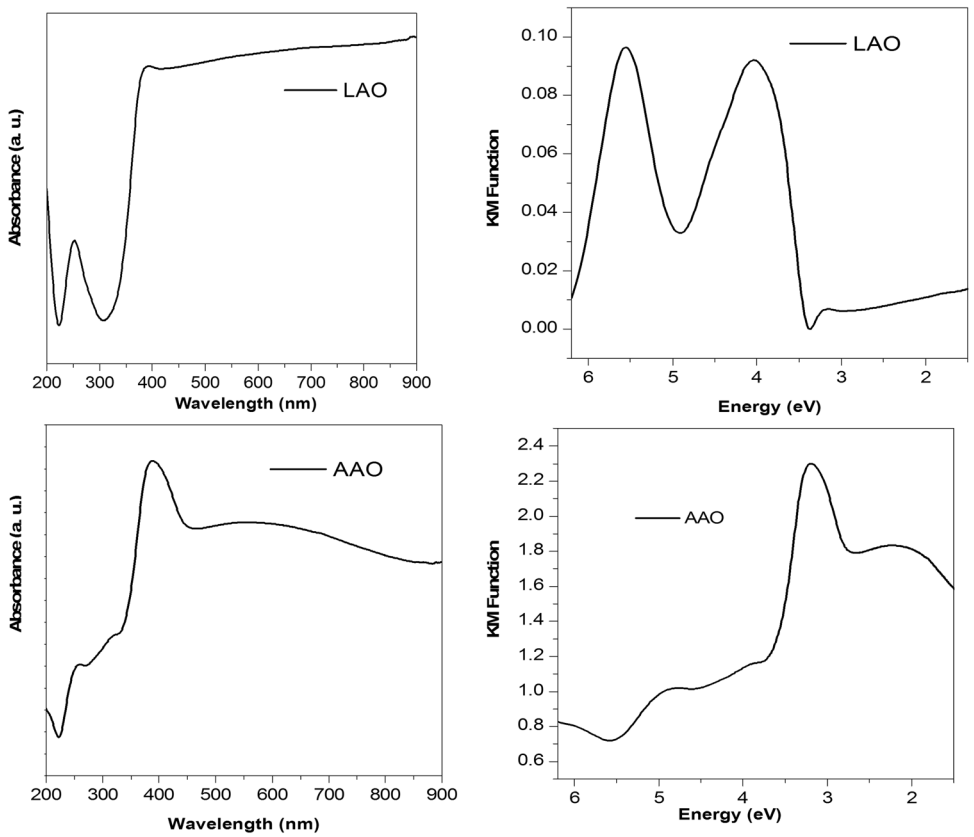

Fig. 4 Absorbance and KM plot of LAO and AAO

energy of LAO and AAO samples is found to be 3.38 and 2.03 eV, respectively.

The photocatalytic activity of LAO and AAO was tested by studying the degradation of methylene Blue (MB) and rhodamine B (RhB) aqueous solutions under visible light irradiation. The degradation of MB and RhB in the presence of LAO was found to be negligible. Figure 5 shows the temporal changes in the concentration of the aforementioned organic dyes in the presence of AAO. The degradation of MB/RhB was measured by following the variations in maximal absorption in the UV–visible spectra at 664/554 nm. Before the irradiation experiments, the samples were kept in the dark chamber for attaining the adsorption–desorption equilibrium. The adsorbed amount of MB and RhB on AAO during the dark reaction was found to be 20 and 7%, respectively. The concentration of MB/RhB decreased with visible light irradiation time. The degraded amount of MB and RhB in 3 h of irradiation was

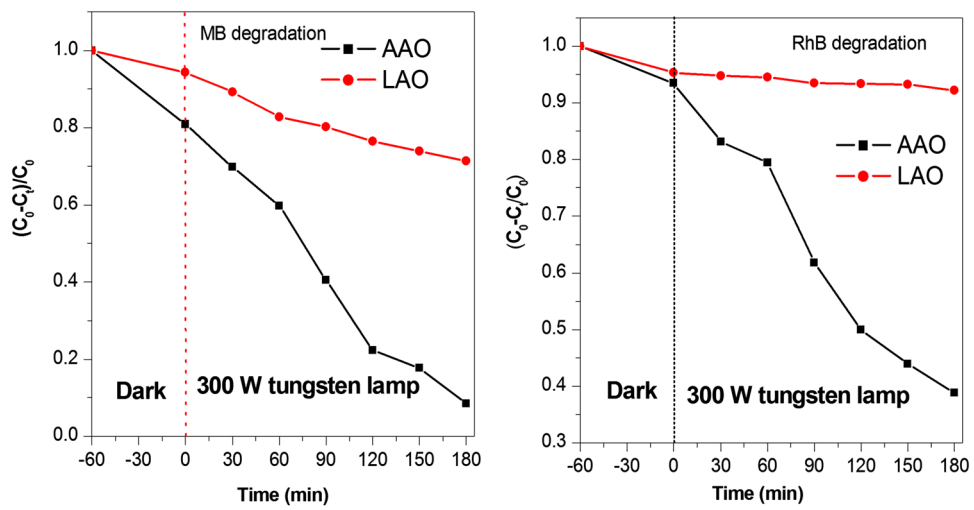

Fig. 5 Temporal changes in the concentration of **a** MB and **b** RhB in the presence of LAO and AAO under the visible light irradiation

about 92 and 63%, respectively (Fig. 5). For semiconductor photocatalytic reactions, light absorption by the material, generation, and migration of light-induced electron–hole pairs are important factors to determine the efficiency of the photocatalyst. The light absorption capacity of the material depends on its bandgap energy. Since the bandgap energy of AAO (2.03 eV) in the visible light region, it absorbs the visible light and generates electron–hole pairs. These electron–hole pairs can migrate to the surface of the semiconductor and combine with surface OH^- species and dissolved oxygen to form the $^{\cdot}OH$ and $O_2^{\cdot-}$, respectively. Subsequently, these OH^- and $O_2^{\cdot-}$ react with dye molecules and degrade them into simple inorganic minerals.

An attempt is made to verify the generation and involvement of these photogenerated holes (h^+), hydroxyl ($^{\cdot}OH$), and superoxide ($O_2^{\cdot-}$) in the RhB degradation process. For this purpose, ammonium oxalate (AO), isopropyl alcohol (*i*-PrOH), and benzoquinone (BQ) were used as radical quenchers to scavenge the holes (h^+), hydroxyl ($^{\cdot}OH$), and superoxide ($O_2^{\cdot-}$) radicals, respectively, during the photodegradation reaction [26–28]. These experiments were carried out as described in Sect. 2.4, but with 2 mM of AO, 2 mM of i-PrOH, and 2 mM of BQ separately under identical experimental conditions (Fig. 6). It is observed from Fig. 6 that the RhB degradation was reduced noticeably by the addition of 2 mM of AO, 2 mM of *i*-PrOH, and 2 mM of BQ to the RhB solution in the presence of the AAO catalyst. The percentage of degradation of RhB after the addition of AO, *i*-PrOH and BQ quenchers was found to be 20, 29 and 35% (it was 62% without AO, *i*-PrOH and BQ separately), respectively. Thus, a decrease in the percentage of degradation of RhB indicates the generation of holes (h^+), hydroxyl ($^{\cdot}OH$), and superoxide ($O_2^{\cdot-}$) species.

The probable mechanism is illustrated below:

$$AAO + hv \rightarrow e_{CB}^- + h_{VB}^+$$
$$OH^- + h_{VB}^+ \rightarrow {}^{\cdot}OH + H^+$$
$$O_2 + e_{CB}^- \rightarrow O_2^{\cdot-}$$
$$O_2^{\cdot-} + {}^{\cdot}OH + RhB \rightarrow Byproducts$$

As stated earlier, LAO has not shown any degradation of MB/RhB under identical conditions (Fig. 4). The bandgap energy of the material and photogenerated electron–hole pairs and their recombination rate play significant role in the photodegradation process. In the present investigation the poor activity of LAO compared to that of AAO can be attributed to (i) wide bandgap energy (3.38 eV), (ii) lower number of electron–hole pairs generated and (iii) higher electron–hole pair recombination rate. The photoluminescence (PL) emission measurements have been widely used to investigate the efficiency of charge carrier migration, trapping, and transfer to understand the fate of electron–hole pairs in semiconductors [29]. It is believed that the higher the intensity of PL signal higher will be electron–hole pair recombination rate. As shown in Fig. 7, the PL intensity in the presence of LAO is maximum indicating higher electron–hole pair recombination rate. Under identical conditions, the PL intensity in the presence of AAO is negligible indicating negligible electron–hole

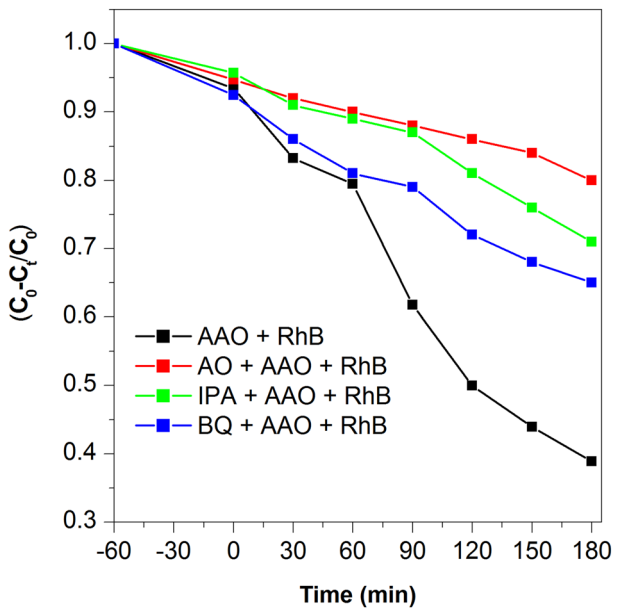

Fig. 6 Photodegradation Rhodamine B with Scavengers in the presence of AAO catalyst

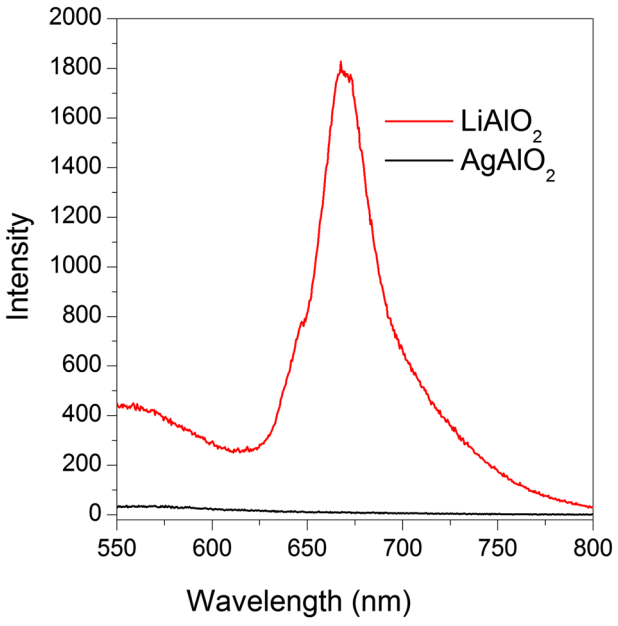

Fig. 7 Photoluminescence spectra of LAO and AAO (excitation wavelength 390 nm)

pair recombination. However, in Fig. 5a, 29% of MB degradation is observed in the presence of LAO. It is due to the self-photolysis of MB in the presence of visible light irradiation [30]. The dissimilarities in the rate of degradation of MB and RhB over AAO may be due to their molecular structure, the extent of ionization in aqueous solution and/or adsorbing capacity of the catalyst [30].

4 Conclusions

$LiAlO_2$ was synthesized by a sol–gel method at 700 °C. $AgAlO_2$ is successfully prepared from the mixture of $LiAlO_2$, $AgNO_3$, and KNO_3. LAO and AAO are crystallized in tetragonal and orthorhombic structures respectively. The bandgap energy of LAO and AAO was found to be 3.38 eV and 2.03 eV respectively. Both the samples have flower-like hierarchical shape particles. The degraded amount of MB and RhB in the presence of AAO was about 92 and 63%, respectively in 3 h of visible light irradiation. The present study indicates that it was feasible to prepare visible light-sensitive semiconductor material by the ion-exchange method and AAO can be used as photocatalyst for the degradation of organic pollutants in an aqueous medium. Based on competitive photocatalytic reactions using scavengers, it was understood that holes (h^+), hydroxyl ($^{\cdot}OH$) radicals and super oxide ($O_2^{\cdot-}$) radicals played a pivotal role in the photocatalytic degradation of RhB. AAO shows higher photocatalytic activity, which can be ascribed to its lower bandgap energy and more charge separation of electron–hole pairs during the photocatalytic process.

Acknowledgements Authors would like to acknowledge the CSIR, New Delhi under the CSIR-scheme (No. 01(2857)/16/EMR-II) for their financial support. MV thanks UGC New Delhi for the award of BSR fellowship.

Compliance with ethical standards

Conflict of interest On behalf of all authors, the corresponding author states that there is no conflict of interest.

References

1. Fujishima A, Rao TN, Tryk DA (2000) Titanium dioxide photocatalysis. J Photochem Photobiol C: Photochem Rev 1:1–21
2. Fox MA, Dulay MT (1993) Heterogeneous photocatalysis. Chem Rev 93:341–357
3. Hoffmann MR, Martin ST, Choi W, Bahnemann DW (1995) Environmental applications of semiconductor photocatalysis. Chem Rev 95:69–96
4. Fujishima A, Honda K (1972) Electrochemical photolysis of water at a semiconductor electrode. Nature 238:37–38
5. Tsuji I, Kato H, Kobayashi H, Kudo A (2004) Photocatalytic H_2 evolution reaction from aqueous solutions over band structure-controlled $(AgIn)_xZn_{2(1-x)}S_2$ solid solution photocatalysts with visible-light response and their surface nanostructures. J Am Chem Soc 126:13406–13413
6. Ouyang S, Li Z, Ouyang Z, Yu T, Ye J, Zou Z (2008) Correlation of crystal structures, electronic structures, and photocatalytic properties in a series of Ag-based oxides: AgAlO2, AgCrO2, and Ag2CrO4. J Phys Chem C 112:3134–3141
7. Chen X, Mao SS (2007) Titanium dioxide nanomaterials: synthesis, properties, modifications, and applications. Chem Rev 107:2891–2959
8. Wei H, Wu Y, Lun N, Zhao F (2004) Preparation and photocatalysis of TiO_2 nanoparticles co-doped with nitrogen and lanthanum. J Mater Sci 39:1305–1308
9. Ni M, Leung MKH, Leung DYC, Sumathy K (2007) A review and recent developments in photocatalytic water-splitting using TiO_2 for hydrogen production. Renew Sustain Energy Rev 11:401–425
10. Nagaraju G, Manjunath K, Ravishankar TN, Ravikumar BS, Nagabhushan H, Ebeling G, Dupont J (2013) Ionic liquid-assisted hydrothermal synthesis of TiO_2 nanoparticles and its application in photocatalysis. J Mater Sci 48:8420–8426
11. Luo Y, Xu Y, Liu X, Xue H, Qian Q, Chen Q (2017) Design of Cu–Ce co-doped TiO_2 for improved photocatalysis. J Mater Sci 52:1265–1271
12. Ravi G, Veldurthi NK, Prasad MD, Munirathnam NR, Prasad G, Vithal M (2013) Preparation, optical, and photocatalytic studies of defect pyrochlores: $KCr_{0.33}W_{1.67}O_6$ and $A_xCr_{0.33}W_{1.67}O_6$ nH_2O. J Nano Part Res 15:1939
13. Hermann JM, Tahiri H, Ait-Ichou Y, Lassaletta G, Gonzalez- Elipe AR, Fernandez A (1997) Characterization and photocatalytic activity in aqueous medium of TiO_2 and Ag–TiO_2 coatings on quartz. Appl Catal B Environ B 13:219–228
14. Kamat PV (2002) Photophysical, photochemical and photocatalytic aspects of metal nanoparticles. J Phys Chem B 106:7729–7744
15. Priyanka V, Yasutaka K, Kohsuke M, Hiromi Y (2017) Enhancement of Ag-based plasmonic photocatalysis in hydrogen production from ammonia borane by the assistance of single-site Ti-Oxide moieties within a silica framework. Chem Eur J 23:3616–3622
16. Jayapandi S, Anitha Prakasini V, Anitha K (2018) Ag modified $LaCoO_3$ perovskite oxide for photocatalytic application. AIP Conf Proc 1942:140048. https://doi.org/10.1063/1.5029179
17. Xiong D, Zeng X, Zhang W, Wang H, Zhao X, Chen W, Cheng Y (2014) Synthesis and characterization of $CuAlO_2$ and $AgAlO_2$ delafossite oxides through low-temperature hydrothermal methods. Inorg Chem 53:4106–4116
18. Fouad OA, Farghaly FI, Bahgat M (2007) A novel approach for synthesis of nanocrystalline γ-$LiAlO_2$ from spent lithium-ion batteries. J Anal Appl Pyrolysis 78:65–69
19. Turner CW, Clatworthy BC, Gin AHY (1988) The preparation of lithium aluminate by the hydrolysis of lithium and aluminium alkoxides. International symposium on fabrication and properties of lithium ceramics, AECL-9614. Adv Ceram 25:141–148
20. Islam MM, Bredow T (2015) Interstitial lithium diffusion pathways in γ -$LiAlO_2$: a computational study. J Phys Chem Lett 2015:4622–4626
21. Ouahdi N, Guillemet S, Durand B, Ouatib RE, Rakho LE, Moussa R, Samdi A (2008) Synthesis of $CoAl_2O_4$ by double decomposition reaction between $LiAlO_2$ and molten $KCoCl_3$. J Eur Ceram Soc 28:1987–1994
22. Shannon RD, Rogers DB, Prewitt CT (1971) Chemistry of noble metal oxides. I. Syntheses and properties of ABO_2. Delafossite Compounds. Inorg. Chem 10:713–718

23. Thompson JG, Withers RL, Palethorpe SR, Melnitchenko A (1998) Cristobalite-related oxide structures. J Solid State Chem 141:29–49
24. Kawazoe H, Yasukawa M, Hyodo H, Kurita M, Yanagi H, Hosono H (1997) P-type electrical conduction in transparent thin films of $CuAlO_2$. Nature 389:939–942
25. Ravi G, Sravan Kumar K, Guje R, Sreenu K, Prasad G, Vithal M (2016) Synthesis, characterization, luminescence and electrical conductivity of the metal ions M doped $KAl_{033}W_{167}O_6$. J Solid State Chem 233:342–351
26. Khodja AA, Sehili T, Pilichowski JF, Boule PJ (2001) Photocatalytic degradation of 2-phenyl phenol on TiO_2 and ZnO in aqueous suspensions. J Photochem Photobiol A: Chem. 141:231–239
27. Zhang Y, Chen Z, Liu S, Xu YJ (2013) Size effect induced activity enhancement and anti-photocorrosion of reduced graphene oxide/ZnO composites for degradation of organic dyes and reduction of Cr(VI) in water. Appl Catal B 140–141:598–607
28. Zhang Y, Zhang N, Tang ZR, Xu YJ (2013) Identification of Bi_2WO_6 as a highly selective visible- light photocatalyst toward oxidation of glycerol to dihydroxyacetone in water. Chem Sci 4:1820–1824
29. Wang E, Zhang P, Chen Y, Liu Z, He T, Cao Y (2012) Improved visible-light photocatalytic activity of titania activated by nitrogen and indium modification. J Mater Chem 22:14443–14449
30. Ravi G, Veldurthi NK, Palla S, Velchuri R, Pola S, Reddy JR, Vithal M (2013) Synthesis, characterization and photocatalytic activity of $KAl_{0.33}W_{1.67}O_6$ and $Sn_{0.5}Al_{0.33}W_{1.67}O_6xH_2O$. Photochem Photobiol 89:824–831